Stress Development in Drying Coatings after Solidification

H. Lei, L. F. Francis, W. W. Gerberich, and L. E. Scriven
Coating Process & Fundamentals Program, Dept. of Chemical Engineering and Materials Science and Center for Interfacial Engineering, University of Minnesota, Minneapolis, MN 55455

As a coating solidifies by drying, it tends to shrink. It is liquid enough in early stages that any shrinkage stress is rapidly relieved by viscous flow. It becomes solid enough in later stages to support elastic stress, which results from shrinkage inhibited by adherence to the substrate. Stress can relax by viscous creep in the coating. Thus, the stress level is an outcome of competing shrinkage and relaxation. A theoretical model of diffusion and mass transfer, large shrinkage-induced deformation and stress, together with yielding and post-yielding viscous deformation, was developed to predict stress evolution in drying of polymer coatings after solidification. The coupled equations of diffusion and stress development are solved by the Galerkin/finite-element method. This model is used in polymer coatings to study the effect of a grooved substrate and embedded particles to the stress and drying, and to simulate cantilever deflection method used to measure stress experimentally.

Introduction

When a liquid coating is applied to a substrate, the viscous stresses that accompany flow quickly relax as the coating comes to rest relative to the substrate. However, the coating may continue to flow a little by gravity, capillary, or air drag forces before it solidifies by chilling, drying, or curing. Upon solidifying, the coating acquires a solid-like nature. Further solvent removal after solidification causes further volume shrinkage and the development of significant stresses.

The development of stress after solidification is due primarily to the inability of in-plane shrinkage by the adhesion of the coating to its substrate (Figure 1a). It is due secondarily to nonuniform shrinkage as the coating dries, although this is equally important at edges (Tam, 1997). In a coating cast from polymer solution, let's assume that, between the reference state at solidification and the current state, there was a stress-free state in which the stress in every infinitesimal domain of the coating was removed. The deformation from the original reference state is purely volume shrinkage in this stress-free state. If the shrinkage was the same everywhere, in every infinitesimal domain, the imaginary stress-free states everywhere would be compatible and the infinitesimal stress-free domains would all fit together at their boundaries. However, the evaporation of solvent through the free surface and the diffusion beneath generally cause nonuniform shrinkage within the coating. For example, in Figure 1b, a block of coating consists of four domains and the amount of shrinkage differs from one to another. For the sake of illustration, each can be taken to be homogeneous. Because they differ in shrinkage, their stress-free states are not compatible, that is, their boundaries can no longer fit to each other. To fit together, each must be strained. As a result, stress is developed provided no cracks or delamination occurs at the junctions between the domains. Actually, stress developed from the hindrance of substrate can be considered as a special case of nonuniform shrinkage in which there is no shrinkage in one "piece" (rigid), and there is shrinkage in the other.

The mechanisms of stress development in shrinkage coatings have long been studied. The interaction of stress and solvent diffusion in solids has been studied by Li and coworkers (Li et al., 1966; Li, 1971) and by Larche and Cahn (1973,

Correspondence concerning this article should be addressed to H. Lei at the following current address: Eastman Kodak Company, Kodak Park, Rochester, NY 14652.

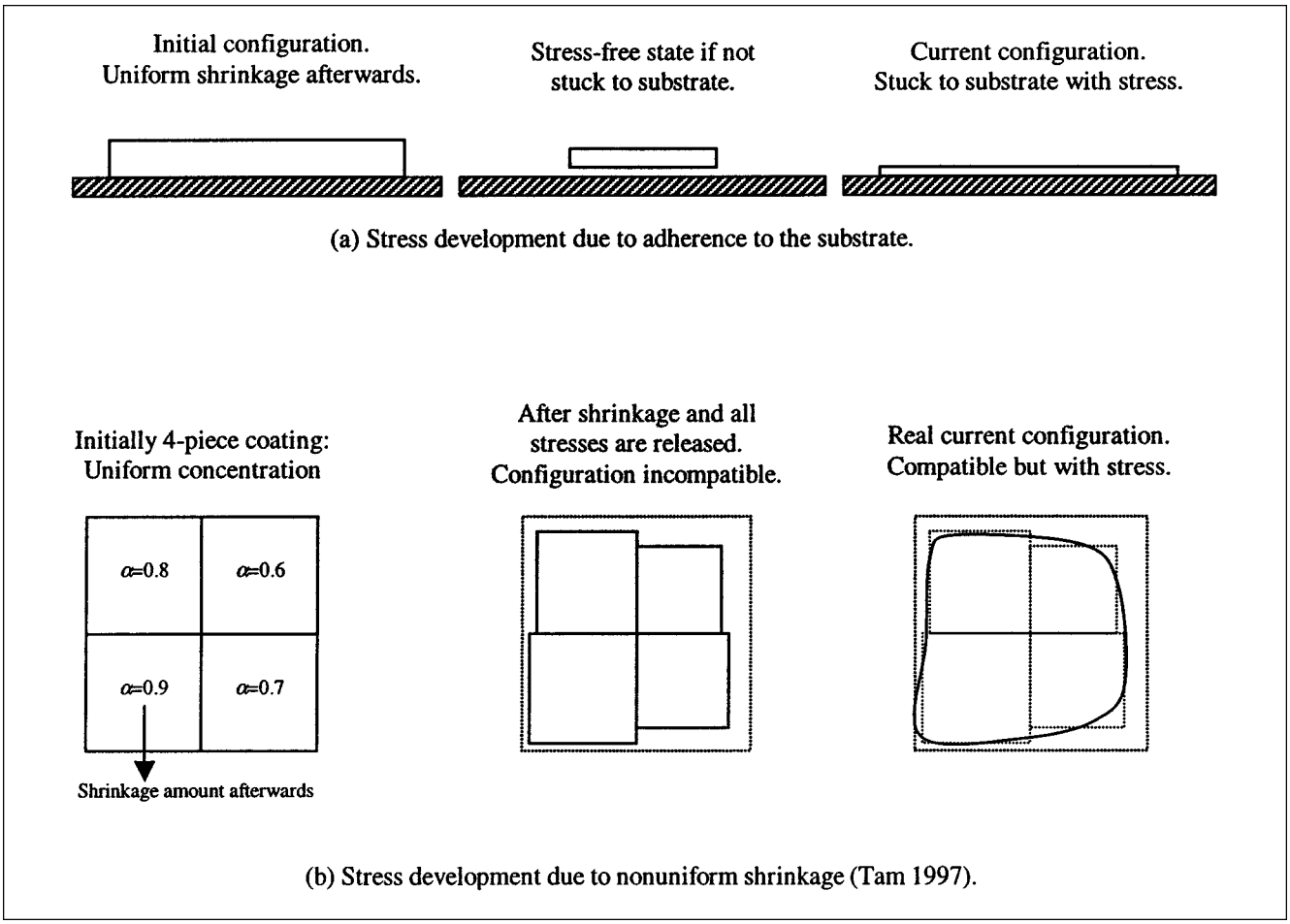

Figure 1. Causes of stress development in solidifying coatings.

(a) Stress development due to adherence to the substrate; (b) stress development due to nonuniform shrinkage.

1982). Both sets of researchers started from a combination of linear elasticity and thermochemical equilibrium to derive the equations. They found that upon linearizing the equation sets, the equations of equilibrium can be separated into purely elastic and purely chemical equations. Later, during the study of clay drying, Hasatani and Itaya (1992) and Hasatani et al. (1993, 1995) used the Galerkin/finite-element method to solve equations of diffusion and the integral form of viscoelastic constitutive equations to simulate shrinkage and stress development. They considered only cases of small deformation in which diffusion and mass transfer can be treated independent of mechanical equilibrium. Wu and Milota (1994) and Irudayaraj and Haghighi (1993) have also studied the creep and viscoelastic drying models under small strain. Recently, Tam and coworkers (Tam et al., 1995; Tam, 1997) were the first to model drying coatings as to account for large deformations, that is, volume shrinkage large enough that linear elasticity is inadequate. They solved the coupled equations of mass transfer from coating to flowing air, diffusion with convection in solvent-polymer layers, and a linear dependence of stress on a quadratic measure of strain. They incorporated yield stress and post-yield viscous deformation, and explored the effect of plastic yielding. In a recent article, Christodoulou and coworkers (1998) also considered the large elastic deformation of a drying gel, in which the non-Fickian diffusion is coupled with the stress taken from a polymer network, as well as an ideal liquid solvent.

This article extends a one-dimensional (1-D) analysis recently developed by Lei et al. (2001) to a full 3-D theoretical analysis that accounts for large elastic strain and stress, as well as viscoplastic straining (nonlinear theory). Unlike other approaches, the constitutive relation used here is appropriate for incompressible elastomeric solids, which most rubbery polymers are. For simplicity and convenience, we disregard the viscous stress from drying liquids, assume that the concentration is uniform at solidification, and focus on the drying after a coating solidifies. The article lays out theory of Fickian diffusion, kinematics of volume shrinkage, elastic deformation, stress development, plastic yielding, and subsequent viscoplastic flow as the solvent evaporates from a polymer solution coating. The coupling of diffusion and stress evolution is solved by the Galerkin/finite-element method. This model is used in polymer coatings to predict the effect of a grooved substrate and embedded particle rigidity on drying and induced stresses after solidification, and to simulate a cantilever deflection method that is being used to measure stress experimentally. To the best of our knowledge, these predictions are novel.

Theory

Drying and diffusion

The evaporation of volatile solvent, the movement of the coating/gas interface, and the solvent diffusion in a coating are described by the principle of conservation of mass. The analysis that follows is of mass transfer in a binary system composed of a volatile solvent and a nonvolatile polymer. Multicomponent systems with two or more solvent species or two or more polymer species can be similarly analyzed. The possibility of chemical reaction changing one species to another is not considered. Volume change upon mixing is also set aside for future analysis.

The species mass conservation (continuity) equations of solvent s and polymer p are

$$\frac{\partial c_s}{\partial t} + \nabla \cdot \boldsymbol{n}_s = 0 \tag{1}$$

$$\frac{\partial c_p}{\partial t} + \nabla \cdot \boldsymbol{n}_p = 0 \tag{2}$$

among which only Eq. 1 needs to be solved due to Amagat's law, or no volume change upon mixing (Cairncross et al., 1992). In Eqs. 1 and 2, c_s and c_p are molar concentrations and $\boldsymbol{n}_s$, $\boldsymbol{n}_p$ are the molar fluxes of solvent and polymer. In the polymer reference coordinate, $\boldsymbol{n}_s$ is split into the solvent convective flux and the diffusive flux relative to the polymer velocity $\boldsymbol{v}_p$

$$\boldsymbol{n}_s = c_s \boldsymbol{v}_s = c_s \boldsymbol{v}_p + \boldsymbol{j}^* \tag{3}$$

in which the diffusive flux (Tam, 1997)

$$\boldsymbol{j}^* = c_s \boldsymbol{v}_s - c_s \boldsymbol{v}_p = -\frac{D}{1 - c_s \bar{V}_s} \nabla c_s \tag{4}$$

D is the binary diffusion coefficient, and $\bar{V}_s$ is the partial molar volume of solvent. The solvent mass conservation equation then becomes

$$\frac{\partial c_s}{\partial t} = -\nabla \cdot (\boldsymbol{j}^* + c_s \boldsymbol{v}_p) \tag{5}$$

Equations 4 and 5 were first derived by Tam (1997). They generalize the polymer reference coordinate long employed in analyses of 1-D Fickian and viscoelastic diffusion (Crank, 1975; Durning, 1986; and Billovits and Durning, 1989). The polymer reference coordinate has been proved to be very successful in simplifying 1-D drying problems, because the convective flux of polymer vanished with it and the troublesome moving boundary problem can be avoided.

Kinematics

To describe how strain evolves in a drying coating, consider how the material deforms and how its stress-free state changes locally as solvent diffuses toward the coating surface and evaporates. Croll (1979) took the original stress-free reference state to be the state of the coating at the instant of solidification, that is, the first appearance of elastic modulus. This is adopted as time $t = 0$. Because only the drying of a coating initially at solidification and with uniform concentration is considered, the initial state ($t = 0$) is stress-free. Each polymer particle in this state can be labeled by its location $\boldsymbol{X}(X_1, X_2, X_3)$ and corresponding Cartesian coordinates (Figure 2). After drying proceeds a time t, the particles are at new positions $\boldsymbol{x}(x_1, x_2, x_3)$, which define the current state. The deformation transformation is

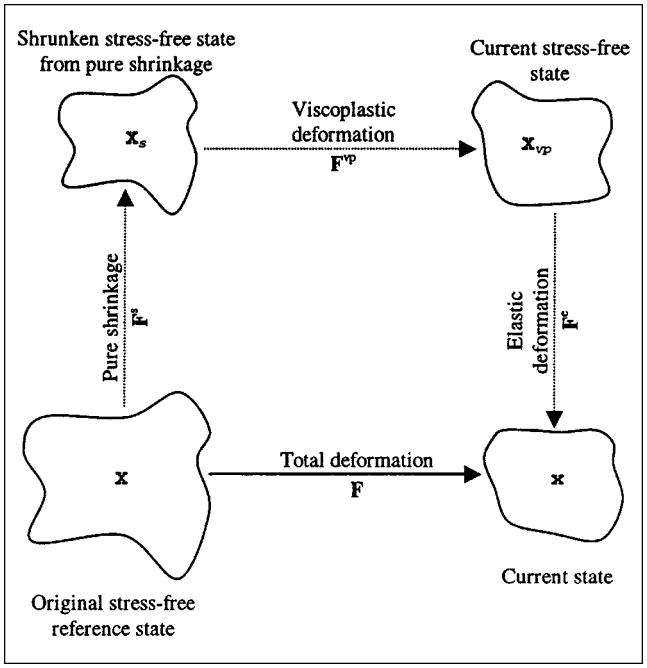

Figure 2. Kinematics of drying elasto-viscoplastic deformation.

The total deformation gradient $\boldsymbol{F}$ from position $\boldsymbol{X}$ in the reference state to position $\boldsymbol{x}$ in the current state is decomposed into three parts, $\boldsymbol{F}^s$, $\boldsymbol{F}^{vp}$, and $\boldsymbol{F}^e$.

$$\boldsymbol{x} = \boldsymbol{x}(\boldsymbol{X};t) = \boldsymbol{X} + \boldsymbol{d}_p(\boldsymbol{X};t) \tag{6}$$

in which $\boldsymbol{d}_p(\boldsymbol{X};t)$ is the displacement of the same polymer particles originally at $\boldsymbol{X}$ and then moved to $\boldsymbol{x}$. This deformation from the initial stress-free state to the current state is described by the deformation gradient

$$\boldsymbol{F} \equiv \nabla_X \boldsymbol{x} \equiv \frac{\partial \boldsymbol{x}}{\partial \boldsymbol{X}} \tag{7}$$

where ∇_X is the gradient operator in the initial stress-free state.

The total deformation from the original reference state to the current deformed state can be decomposed into three successive deformation steps (Lee, 1969; Tam, 1997):

(1) Volume shrinkage from the original stress-free state $\boldsymbol{X}$ to an intermediate stress-free state $\boldsymbol{X}_s$

(2) Viscous flow and plastic deformation, if the coating yields locally, from this shrunken intermediate stress-free state $\boldsymbol{X}_s$ to the current stress-free state $\boldsymbol{X}_{vp}$

(3) Elastic deformation from this current stress-free state $\boldsymbol{X}_{vp}$ to the current actual state $\boldsymbol{x}$.

This decomposition of total deformation into three individual parts is shown in Figure 2. Normally, if the boundary constraints in the current state are removed, a residual stress distribution will remain following nonuniform shrinkage and/or nonhomogeneous viscoplastic flow. To completely remove the residual stress, the coating will have to be cut into small elements and the corresponding configurations $\boldsymbol{X}_s$ and $\boldsymbol{X}_{vp}$ will be discontinuous. For the case when the configurations $\boldsymbol{X}_s$ and $\boldsymbol{X}_{vp}$ are continuous and differentiable, the total deformation gradient $\boldsymbol{F}$ can be multiplicatively decomposed into the shrinkage gradient $\boldsymbol{F}^s$, viscoplastic deformation gradient $\boldsymbol{F}^{vp}$, and elastic deformation gradient $\boldsymbol{F}^e$ according to the chain rule for partial differentiation

$$\boldsymbol{F} = \boldsymbol{F}^e \cdot \boldsymbol{F}^{vp} \cdot \boldsymbol{F}^s \tag{8}$$

Whenever the stress free states $\boldsymbol{X}_s$ and $\boldsymbol{X}_{vp}$ are discontinuous, the deformation gradients $\boldsymbol{F}^s$, $\boldsymbol{F}^{vp}$, and $\boldsymbol{F}^e$ reduce to tensors of local linear mappings in the limit of small material elements, which also satisfy Eq. 8 but not the continuity conditions for partial derivatives (Lee, 1969).

The shrinkage from the original stress-free state to the intermediate shrunken stress-free state is generally isotropic and thus

$$\boldsymbol{F} = \boldsymbol{F}^e \cdot \boldsymbol{F}^{vp} \alpha \tag{9}$$

where α is a shrinkage ratio that describes the amount of volume shrinkage. The only volume change here is that as solvent evaporates. By hypothesis, specific volumes are additive and Amagat's law applies to the solution; this gives

$$\alpha = \left(\frac{dv}{dV} \right)^{1/3} = \left(\frac{1 - c_s^0 \overline{V}_s}{1 - c_s \overline{V}_s} \right)^{1/3} = \left(\frac{1 - f_s^0}{1 - f_s} \right)^{1/3} \tag{10}$$

where dv is the current derivative equilibrium volume per unit of polymer with solvent concentration c_s, and dV is the initial derivative equilibrium volume per unit of polymer with concentration c_s^0; f_s^0 and f_s are, respectively, the initial and current volume fractions of solvent.

The elastic deformation from the current stress-free state to the current state is described by the gradient tensor $\boldsymbol{F}^e$. The corresponding elastic strain relative to the locally current stress-free state can be expressed as either the left or right Cauchy-Green tensors (Malvern, 1969)

$$\boldsymbol{B}^e = \boldsymbol{F}^e \cdot \boldsymbol{F}^{e^T} \qquad \boldsymbol{C}^e = \boldsymbol{F}^{e^T} \cdot \boldsymbol{F}^e \tag{11}$$

The superscript "T" denotes the transpose. Any difference between the current stress-free state and the current state causes $\boldsymbol{B}^e$ and $\boldsymbol{C}^e$ to derivate from the identity tensor $\boldsymbol{I}$; such deviation gives rise to stress.

To analyze the rate-dependent viscoplastic behavior, the material gradient of velocity $\boldsymbol{L}$ is calculated such that (Malvern, 1969)

$$\boldsymbol{L} \equiv \nabla \boldsymbol{v}_p = \dot{\boldsymbol{F}} \cdot \boldsymbol{F}^{-1} = \boldsymbol{L}^e + \boldsymbol{F}^e \cdot \boldsymbol{L}^{vp} \cdot \boldsymbol{F}^{e^{-1}} + \frac{\dot{\alpha}}{\alpha} \boldsymbol{I} \tag{12}$$

where a dot above the tensor stands for the polymer particle material time derivative. In Eq. 12, ∇ is the gradient operator in the current state; $\boldsymbol{L}^e$ and $\boldsymbol{L}^{vp}$ are the elastic and the viscoplastic velocity gradients in the current state, which are given by

$$\boldsymbol{L}^e = \dot{\boldsymbol{F}}^e \cdot \boldsymbol{F}^{e^{-1}} \qquad \text{and} \qquad \boldsymbol{L}^{vp} = \dot{\boldsymbol{F}}^{vp} \cdot \boldsymbol{F}^{vp^{-1}} \tag{13}$$

The polymer velocity gradient $\boldsymbol{L}$ is expressed in the current state. However, because the elastic strain tensor, and, thus, the stress tensor, is evaluated relative to the current stress-free state, the polymer material derivatives in Eq. 12 need to be transformed to the current stress-free state (Moran et al., 1990; Tam, 1997) to obtain

$$\overline{\boldsymbol{L}} = \boldsymbol{F}^{e^T} \cdot \boldsymbol{L} \cdot \boldsymbol{F}^e = \overline{\boldsymbol{L}}^e + \overline{\boldsymbol{L}}^{vp} + \frac{\dot{\alpha}}{\alpha} \boldsymbol{C}^e \tag{14}$$

with the overbar indicating they are expressed in the current stress-free state. In Eq. 14

$$\overline{\boldsymbol{L}}^e = \boldsymbol{F}^{e^T} \cdot \dot{\boldsymbol{F}}^e, \qquad \overline{\boldsymbol{L}}^{vp} = \boldsymbol{C}^e \cdot \dot{\boldsymbol{F}}^{vp} \cdot \boldsymbol{F}^{vp^{-1}} \tag{15}$$

are the elastic and the viscoplastic parts of the velocity gradient in the current stress-free state. The symmetric parts of $\overline{\boldsymbol{L}}^e$ and $\overline{L}^{vp}$ are denoted $\overline{\boldsymbol{D}}^e$ and $\overline{\boldsymbol{D}}^{vp}$, respectively

$$\overline{\boldsymbol{D}}^e \equiv \frac{1}{2} (\overline{\boldsymbol{L}}^e + \overline{\boldsymbol{L}}^{e^T}), \qquad \overline{\boldsymbol{D}}^{vp} \equiv \frac{1}{2} (\overline{\boldsymbol{L}}^{vp} + \overline{\boldsymbol{L}}^{vp^T}) \tag{16}$$

$\overline{\boldsymbol{D}}^e$ and $\overline{\boldsymbol{D}}^{vp}$ are interpreted as the elastic and viscoplastic strain rates [they are called the rates of deformation in the stress-free state by Malvern (1969)]. The viscoplastic strain rate is used in describing viscoplastic behavior whose constitutive equation is expressed in terms of the stresses.

Equation of equilibrium

Before a coating solidifies, the liquid can easily flow. After solidification, because material moves slowly with respect to the substrate in coatings, drying can be considered a quasi-static process in which the inertia is negligible. Ordinarily, the effect of gravity is also negligible. For instance, if the acceleration rate is 0.01 m/s^2, the inertia term has a magnitude of 10 N/m^3. For a coating about 100 μm in thickness, the pressure due to the gravity is about 1 N/m^2. However, if the polymer is in the glassy state and the relaxation rate of the polymer is much slower than the drying rate, the stress that develops usually exceeds 10^6 N/m^2. Thus, the inertia and gravity terms can safely be neglected and the Cauchy momentum balance is simply

$$\nabla \cdot \sigma = 0 \tag{17}$$

The Cauchy equation of motion (Eq. 17) applies to the current state. The Cauchy stress tensor field σ is defined as a function of the current "particle" positions $\boldsymbol{x}$, and it is a symmetric tensor. A suitable strain measure to use with the

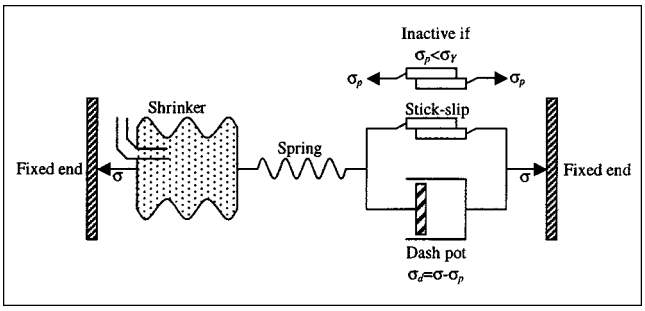

Figure 3. Basic 1-D shrinking elasto-viscoplastic model.

Cauchy stress tensor would therefore be one of the strain or deformation tensors of the spatial formulation in terms of the current particle position.

Constitutive equations

The concept of elasto-viscoplastic behavior in shrinking coatings is best introduced by means of the 1-D rheological model illustrated in Figure 3. The idea is to use different models to describe the various deformations as in Figure 2. The "shrinker" unit accounts for the isotropic volume shrinkage, which, in this 1-D model, reduces its length by solvent removal or chemical reaction. In the case of an ideal solution, the amount of shrinkage (length reduction) is related to the amount of solvent loss or the extent of reaction. The "shrinker" responds instantaneously upon any change in coating composition or in chemical reaction. The "spring" represents the elastic behavior of the coating. For a Hookean solid, stress is proportional to the modulus and the elastic strain from the stress free state. The "spring," like the "shrinker," also responds without delay upon any change in elastic strain. A "dash pot" and a "stick-slip" in parallel introduce the viscoplastic behavior. The "dash pot" describes viscous flow, creep, and relaxation behavior in the coating, and it is a strain rate-dependent unit on which the rate of strain is related to the stress. The "stick-slip" unit accounts for the yielding and viscoplastic flow behavior in which the stress level depends on whether or not the threshold or yield stress σ_Y has been reached. The onset of viscoplastic deformation is governed by a uniaxial yield stress σ_Y. The stress level for continuing viscoplastic flow depends on the strain-hardening characteristics of the material.

Constitutive equations for 3-D elasto-viscoplastic models are complicated because stress and strain are dyadics or tensors. In general, due to the stress and strain, the elastic behavior of coating depends on the solvent concentration, the Cauchy-Green deformation tensors, and the history of plastic deformation. Tam (1997) used a linear relation of the stress and a quadratic measure of strain to describe the elastic response. In this study the material, by hypothesis, follows the neo-Hookean (Rivlin and Saunders, 1951) constitutive equation

$$\sigma = -\pi \boldsymbol{I} + G\boldsymbol{B}^e \tag{18}$$

in which G is the solvent-concentration dependent shear modulus and π is the hydrostatic pressure.

The neo-Hookean equation is for incompressible materials and is a fair approximation for polymer-solvent systems in the rubbery state, which are generally incompressible. It is used here to model polymer solutions that solidify by gelling and by vitrifying. This approximation becomes less robust in the latter case, because glass polymers become somewhat compressible as their glass transition temperature rises (due to solvent departure) above the experimental temperature. The condition of incompressibility in elastic deformation is

$$\det(\boldsymbol{F}^e) = 1 \tag{19}$$

Elasto-viscoplastic behavior is characterized by an elastic material response at low stress onto which a viscoplastic deformation begins after a certain level of stress has been reached. As the drying continues and the stress rises, some parts of the coating enter a viscoplastic regime. The onset of plastic deformation (or yielding) is governed by the yield criterion. The time-rate effects after yielding is modeled by the viscoplastic theory. This study only considers ideal isotropic viscoplastic materials with no strain hardening. It is also assumed that plastic deformation does not produce any volume change. The model, first developed by Moran et al. (1990), is based on the yield surface in the stress space described by Von Mises' criterion. In using the Von Mises' criterion, the second Piola-Kirchhoff stress tensor on the current stress-free state $\bar{\boldsymbol{S}}$ is given by the mapping of the Cauchy stress on the current state to the current stress-free state

$$\bar{\boldsymbol{S}} = (\det \boldsymbol{F})\boldsymbol{F}^{e^{-1}} \cdot \sigma \cdot \boldsymbol{F}^{e^{-T}} \tag{20}$$

The deviatoric part of this in the current stress-free state is

$$\bar{\boldsymbol{S}}' = \bar{\boldsymbol{S}} - \frac{1}{3}(\bar{\boldsymbol{S}}:\boldsymbol{C}^e)\boldsymbol{C}^{e^{-1}} \tag{21}$$

The second invariant of $\bar{\boldsymbol{S}}'$ is

$$\Phi = \sqrt{\frac{1}{2}(\bar{\boldsymbol{S}}'^T \cdot \boldsymbol{C}^e):(\bar{\boldsymbol{S}}' \cdot \boldsymbol{C}^{e^T})} \tag{22}$$

The Von Mises' yield criterion can then be expressed as

$$\boldsymbol{\Phi} - k = 0 \tag{23}$$

where k is the critical shear stress at yielding and acts to define the "size" of the abstract yield surface in the space of principal stresses.

The simplest choice of a constitutive relation for the viscoplastic strain rate in Eq. 16 is that of Owen and Hinton (1980) and Lubliner (1990)

$$\bar{\boldsymbol{D}}^{vp} = \frac{1}{\mu}\langle \Phi - k \rangle \frac{\partial \Phi}{\partial \bar{\boldsymbol{S}}} \tag{24}$$

where μ is the post-yield viscosity of the stress-free state. In Eq. 24, the viscoplastic strain rate is proportional to the excess stress above the yield surface. In the abstract space, the

viscoplastic strain rate has a direction normal to the yield surface. The notation $\langle\ \rangle$ implies

$$\langle \Phi - k \rangle = \begin{cases} \Phi - k & \text{if } \Phi > k \\ 0 & \text{otherwise} \end{cases} \tag{25}$$

In Cartesian coordinates, Eq. 24 gives the components of viscoplastic strain rate as

$$\bar{D}^{vp}_{MN} = \frac{1}{2\mu} \frac{\langle \Phi - k \rangle}{\Phi} C^e_{IM} C^e_{JN} \bar{S}'_{IJ} \tag{26}$$

in which the Einstein notation of summation has been used; C^e_{IM}, $\bar{S}'_{IJ}$, and $\bar{D}^{vp}_{MN}$ are components of $\boldsymbol{C}^e$, $\bar{\boldsymbol{S}}'$, and $\bar{\boldsymbol{D}}^{vp}$, respectively. The flow rule in Eq. 26 provides only the symmetric part of viscoplastic velocity gradient $\bar{L}^{vp}$ in Eq. 15. According to Dafalias (1985), the antisymmetric part (also known as plastic spin) is important only on a microscopic scale if at all.

Boundary conditions

At the coating/substrate interface, the polymer adheres to the substrate and moves with it. Exceptions are when the coating delaminated from the substrate, and these exceptions are not considered here. Many coatings, even when solidified, are a lot softer than the substrates they are coated on. When the substrate can be regarded as rigid, the polymer displacement along the substrate should vanish

$$\boldsymbol{d}_p = \boldsymbol{0}, \text{ at coating/rigid substrate interface} \tag{27}$$

If the substrate is flexible, the displacement at the coating/substrate interface becomes one part of the solution, as in the cantilever deflection problem that will be discussed later.

At the free surface of the coating, there is no traction

$$\hat{\boldsymbol{n}} \cdot \sigma = \boldsymbol{0} \tag{28}$$

Here, $\hat{\boldsymbol{n}}$ is the normal vector at the free surface pointing from the coating to the air.

Another kind of boundary condition that will be used in the following examples is the symmetric boundary condition. This condition requires that the polymer material moves only along the symmetric plate, and that the normal derivatives of any variables vanish.

Boundary conditions for drying equations at the free surface are the continuity of mass flux of volatile solvent

$$\hat{\boldsymbol{n}} \cdot \boldsymbol{j}^* = k_g^0 \left(H c_s - c_g^{\text{eq}} \right) \tag{29}$$

where the molar flux on the air side is described by a mass-transfer coefficient k_g^0 multiplied by a concentration difference driving force, H is Henry's coefficient, Hc_s is the solvent concentration in the gas at the surface and in equilibrium with that in the liquid at the surface, and c_g^{eq} is the solvent concentration in the gas far from the surface.

At the coating/substrate interface, provided that the substrate is impermeable to both solvent and polymer, the mass flux should disappear

$$\hat{\boldsymbol{n}} \cdot \boldsymbol{j}^* = 0 \tag{30}$$

where $\hat{\boldsymbol{n}}$ is the unit vector normal to the coating/substrate interface and points from the coating to the substrate.

Galerkin/Finite Element Solution

In polymer-solvent systems, the diffusion coefficient is a strong function of concentration

$$D = D_0 e(c_s) \tag{31}$$

where $e(c_s)$ is a monotonically rising function of solvent concentration. Mechanical properties, which appear after solidification, also depend on solvent concentration. Shear modulus, yield stress, and postyield viscosity can be expressed as products of terminal values and functions of solvent concentration

$$G = G_0 g(c_s),\ \mu = \mu_0 m(c_s),\ k = k_0 n(c_s) \tag{32}$$

Before solving the governing equations by numerical methods, they are nondimensionalized. The variables are also changed to dimensionless variables. In this way the variables are measured in units that make them of the order of unity or less.

The dimensionless solvent volume fraction, as defined in Table 1, is used to evaluate the solvent concentration. The characteristic physical length L (such as initial film thickness) is used to measure length. $T \equiv L^2/D_0$ is taken to measure time. To simplify the momentum equation, to simplify the constitutive equation, and to make the stress the order of unity, the terminal shear modulus G_0 is used to measure the stress. With these characteristic dimensions, the nondimensional governing equations are

$$\text{Continuity:} \quad \frac{\partial f_s}{\partial \tau} = -\bar{\nabla} \cdot \left(\bar{\boldsymbol{j}}^* + f_s \bar{\boldsymbol{v}}_p \right) \tag{33}$$

$$\text{Momentum balance:} \quad \bar{\nabla} \cdot \bar{\sigma} = \boldsymbol{0} \tag{34}$$

$$\text{Incompressibility:} \quad \det(\boldsymbol{F}^e) = 1 \tag{35}$$

The basic unknowns of the governing equations are volume fraction of solvent, polymer displacement, and hydrostatic

Table 1. Dimensionless Variables and Parameters

Time $\tau = D_0 t/L^2$	Gradient operator $\bar{\nabla} = L\nabla$
Solvent vol. fraction $f_s = c_s \bar{V}_s$	Pressure $\bar{\pi} = \pi/G_0$
Init. solvent vol. fraction $f_s^0 = c_s^0 \bar{V}_s$	Equil. solvent vol. fraction $f_s^{\text{eq}} = c_g^{\text{eq}} \bar{V}_s/H$
Polymer displacement $\bar{\boldsymbol{d}}_p = \boldsymbol{d}_p/L$	Polymer flux $\bar{\boldsymbol{j}}^* = \boldsymbol{j}^*/(D_0/L\bar{V}_s) = -[e/(1-f_s)]\bar{\nabla} f_s$
Particle position $\bar{\boldsymbol{X}} = \boldsymbol{X}/L$, $\bar{\boldsymbol{x}} = \boldsymbol{x}/L$	Sherwood no. $Sh = k_g^0 LH/D_0$
Polymer velocity $\bar{\boldsymbol{v}}_p = \boldsymbol{v}_p/(D_0/L)$	Elasticity no. $N_{El} = G_0 L^2/\mu_0 D_0$
Stress tensor $\bar{\sigma} = \sigma/G_0$	Yield stress $\kappa = k_0/G_0$

pressure. The variables and parameters shown above are defined in Table 1. With these dimensionless parameters, the boundary conditions (Eqs. 27–30) become

$$\bar{\boldsymbol{d}}_p = \mathbf{0} \qquad \text{at coating/rigid substrate interface} \tag{36}$$

$$\hat{\boldsymbol{n}} \cdot \bar{\sigma} = \mathbf{0} \qquad \text{at the free surface} \tag{37}$$

$$\hat{\boldsymbol{n}} \cdot \dot{\boldsymbol{j}}^* = Sh\left(f_s - f_s^{\mathrm{eq}}\right) \qquad \text{at the coating/air interface} \tag{38}$$

$$\hat{\boldsymbol{n}} \cdot \dot{\boldsymbol{j}}^* = 0 \qquad \text{at the coating/substrate interface} \tag{39}$$

To solve for the unknowns, the combination of the method of subdomains, Galerkin's method, and finite element basis functions (known as the method of finite elements) are applied to the above set of equations.

Multiplying Eq. 34 by a set of weighting functions ϕ_i ($i = 1, \ldots, N$) and integrating it over the current domain Ω yields the weak form of the momentum balance equation

$$\boldsymbol{R}_i^m = \int_\Omega \left(\bar{\nabla} \cdot \bar{\sigma}\right) \phi_i d\Omega = \mathbf{0}. \tag{40}$$

Integrating the above equation by parts and applying the divergence theorem to the stress term gives

$$\boldsymbol{R}_i^m = -\int_\Omega \bar{\sigma} \cdot \bar{\nabla} \phi_i d\Omega + \int_S \hat{\boldsymbol{n}} \cdot \bar{\sigma} \phi_i dS \tag{41}$$

where S is the control surface containing the current domain Ω; $\hat{\boldsymbol{n}}$ is the outward unit vector normal to the surface S. The integral over the surface of the current domain in Eq. 41 is conveniently evaluated by separately considering the coating/air interface and the coating/substrate interface. The surface integral over the coating/air interface vanishes according to the traction free boundary condition (Eq. 37).

The weak form of the solvent mass-transfer equation in the current configuration is

$$\begin{aligned} R_i^c &= \int_\Omega \left[\frac{\partial f_s}{\partial \tau} + \bar{\nabla} \cdot \left(\dot{\boldsymbol{j}}^* + f_s \bar{\boldsymbol{v}}_p \right) \right] \phi_i d\Omega \\ &= \int_\Omega \left[\left(\frac{d_m f_s}{d\tau} - \bar{v}_p \cdot \bar{\nabla} f_s \right) \phi_i - \left(\dot{\boldsymbol{j}}^* + f_s \bar{\boldsymbol{v}}_p \right) \cdot \bar{\nabla} \phi_i \right] d\Omega \\ &\qquad + \int_S \hat{\boldsymbol{n}} \cdot \left(\dot{\boldsymbol{j}}^* + f_s \bar{\boldsymbol{v}}_p \right) \phi_i dS \\ &= 0 \end{aligned} \tag{42}$$

In Eq. 42 the divergence term has been integrated by parts. The natural flux boundary condition at the coating/air interface and the impermeable boundary condition at the coating/substrate interface are readily applied. In Eq. 42, the local rate of change in f_s is replaced by its time derivative (with respect to the polymer) by using the relation between the time derivative with respect to the frame moving with polymers $d_m/d\tau$ and the local rate of change $\partial/\partial\tau$

$$\frac{d_m f_s}{d\tau} = \frac{\partial f_s}{\partial t} + \bar{v}_p \cdot \bar{\nabla} f_s \tag{43}$$

The weighted residual of the incompressible condition in the current configuration is

$$R_i^\pi = \int_\Omega (\det \boldsymbol{F}^e - 1) q_i \, d\Omega = 0 \tag{44}$$

where q_i are scalar weighting functions which can be different from ϕ_i. Equation 44 provides the equation for the unknown pressure field.

In Galerkin's method, the unknown fields (here $\bar{d}_{px}$, $\bar{d}_{py}$, f_s, $\bar{\pi}$) are represented by the same basis functions that are used as the weighting functions. For example, the displacements and concentration can be represented by

$$\bar{d}_{px} = \sum_{j=1}^{n} \bar{d}_{pxj} \phi_j, \quad \bar{d}_{py} = \sum_{j=1}^{n} \bar{d}_{pyj} \phi_j, \quad f_s = \sum_{j=1}^{n} f_{sj} \phi_j \tag{45}$$

Here the $\phi_j (j = 1, \ldots, n)$ are scalar basis functions and $\bar{d}_{pxj}$, $\bar{d}_{pyj}$, f_{sj} are their coefficients, which are unknowns at this stage. The hydrostatic pressure field can be represented by

$$\bar{\pi} = \sum_{j=1}^{m} \bar{\pi}_j q_j \tag{46}$$

where $q_j (j = 1, \ldots, m)$ are scalar basis functions which are the same as those weighting functions used for the incompressibility condition, and the $\bar{\pi}_j$ their coefficients which are also unknowns. In this work, each component of the scalar basis functions $\phi_j (j = 1, \ldots, n)$ is a continuous, biquadratic polynomial that is non-zero only over a small portion of the domain, and the scalar basis functions $q_j (j = 1, \ldots, m)$ are piecewise, discontinuous, linear polynomials that are likewise non-zero only over a small part of the domain.

Once the field variables are represented in terms of the basis functions, the system of partial differential equations becomes differential-algebraic equations for the coefficients of the basis functions. After a finite difference scheme is applied to approximate the time derivatives, this set of differential-algebraic equations becomes simultaneous algebraic equations, which are nonlinear and sparse. The solution is obtained by Newton's method, which requires evaluation of the full Jacobian matrix. Finite difference formulas are used here to evaluate the components of the Jacobian matrices.

For the predictions in the next section, the coating properties D, G, μ, and k were taken to be independent of concentration; so were the Henry's law coefficient H and the mass-transfer coefficient k_g. To trace the time dependence of concentration and displacements, a time integration scheme is required for the residual equations. The most simple time integration schemes are forward difference and backward difference schemes, and the backward difference scheme is applied here. Within each time increment, the Newton-Raphson iteration method is used to obtain the converged solution. Within each iteration, the Von Mises' yield criterion is checked at each nodal point. If the material doesn't yield locally, the local viscoplastic deformation gradient doesn't change from the previous time increment. On the other hand, if the coating yields locally, Eqs. 16 and 26 are solved for the current viscoplastic deformation gradient by using the backward time difference scheme.

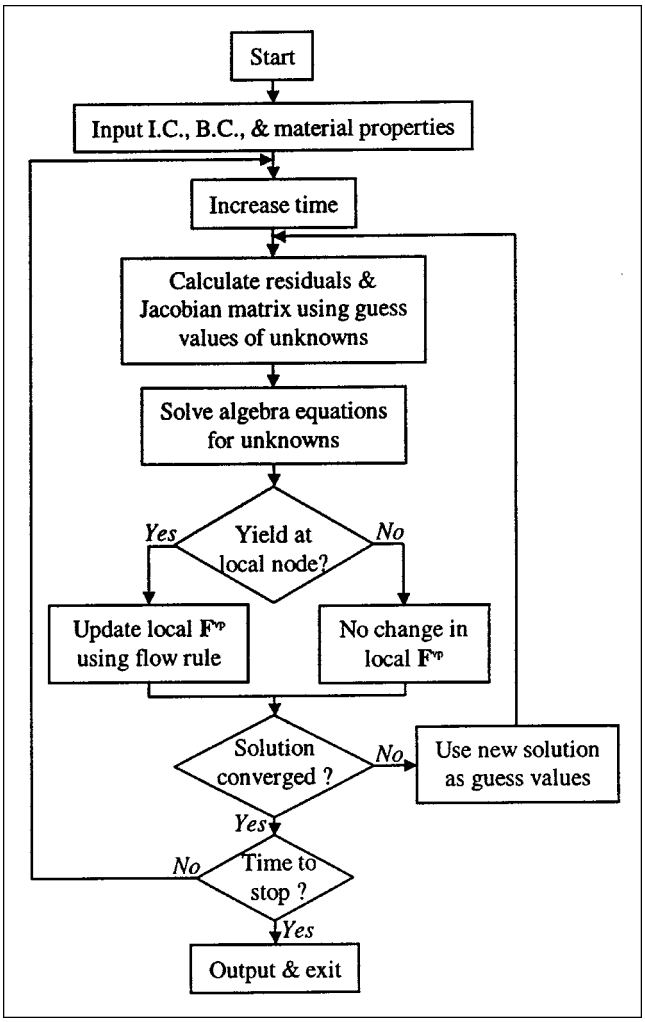

Figure 4. Program about drying and stress development.

I.C. = initial conditions; B.C.-boundary conditions.

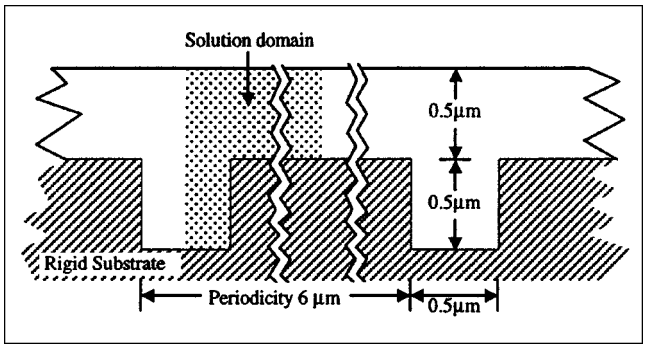

Figure 5. Example used to analyze drying coating on an uneven substrate.

The characteristic length of 1 μm was chosen as unit of length in dimensional analysis.

Results and Discussion

A FORTRAN program (Lei, 1999) was designed based on the above analysis for 2-D drying and stress development under plane-strain conditions. The flow chart of the program is shown in Figure 4. Several examples of this analysis are presented in the following sections.

Coating over a grooved substrate

In industrial coating processes, polymer solutions are sometimes applied to an uneven surface. Examples are photoresist films in microlithography and dielectric layers of multilevel devices. When a polymer solution is cast over a rough surface, the solution flows before it solidifies. However, as more solvent evaporates and the coating undergoes solidification, it becomes more solid like and able to support elastic deformation. This is shown in the spin coating when a polymer/solvent solution is poured onto an uneven substrate and then accelerated to a spin speed of several thousand revolutions per minute. Experimental work on coating (especially spin-coating) over uneven topography was reported by Peurrung and Graves (1991), White (1983), Vergne and Hofer (1985), and Wilson and Piacente (1986). Their studies focused primarily on measurements of dry film profiles.

Prediction of the surface profile while coating over an uneven substrate has been reported by Bornside (1988, 1990). He considered the local planarization of rough surfaces by drying of spin-coated polymer/solvent solutions. A polymeric coating is considered in his model to be a Newtonian fluid with its viscosity depending on solvent concentration.

Unlike Bornside's effort in coupling drying and Newtonian flow, the following results are the predictions on the evolution of surface profiles, solvent concentration, and stresses in the drying of a solid-like coating subjected to plane strain conditions. Before the coating solidifies, the solution is considered as a liquid and can flow. Therefore, at solidification, the coating/air surface is flat. Surface profiles after solidification are controlled by how the polymer moves at the coating/air interface, which is dictated by the evaporation of volatile solvent and mechanical deformation of solid-like coatings to keep it under mechanical equilibrium.

In this example, the coating at solidification is on a substrate with periodic long grooves that go into the paper, as shown in Figure 5. The dimensions of these grooves are 0.5 μm deep by 0.5 μm wide, which is comparable with the coating thickness relative to the ungrooved substrate at solidification (0.5 μm) and the periodicity of the grooves (6 μm). When the drying takes place uniformly on all coating surfaces in contact with the overlying air, only one-half of a period needs to be analyzed. Solvent concentration and stress at other places are available through symmetric conditions. At solidification, the domain chosen is discretized into a mesh of 220 biquadratic nine-node elements, shown in Figure 6 together with the mesh position and the polymer displacement plots after drying of one unit dimensionless time.

Figure 7 shows the concentration contours at five intermediate times. In the early stage of drying the concentration gradient is significant only close to the free surface. The concentration contours and surface profile show little effect on the presence of the groove, as is shown at $\tau = 0.02$ in Figure 7. However, as drying proceeds, the presence of the groove has a dramatic effect. The groove acts as a reservoir of solvent, because the thicker coating over the groove dries more

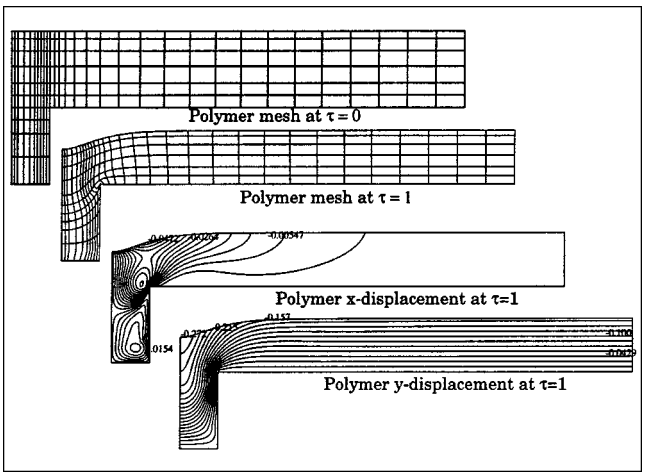

Figure 6. Drying coating over an uneven substrate: the mesh position at solidification and mesh position after $\tau = 1$ of drying.

Displacement contour plots are also shown at $\tau = 1$. Parameters are $f_s^0 = 0.3$, $f_s^{eq} = 0$, $Sh = 5$, $\Delta\tau = 0.01$, $k/G = \infty$.

slowly and sets up a large lateral concentration gradient. As volatile solvent diffuses down the concentration gradient to the regions of lower solvent concentration, the nonvolatile polymer network also moves and deforms due to the volume change in the coating.

The contour plots of dimensionless hydrostatic pressure π/G and Cauchy stress components σ_{xx}/G, σ_{xy}/G, σ_{yy}/G, σ_{zz}/G at $\tau = 1$ are shown in Figure 8. The local smoothing technique of Lee et al. (1979) has been applied to these contour plots. The hydrostatic pressure and all Cauchy stress components shown are concentrated at the tips where the grooves are located. This is due to the sharp change in geometry there. At $\tau = 1$, only about 0.2 vol. % of solvent is left and the coating is almost dried. Far away from the groove, stresses are almost uniformly distributed.

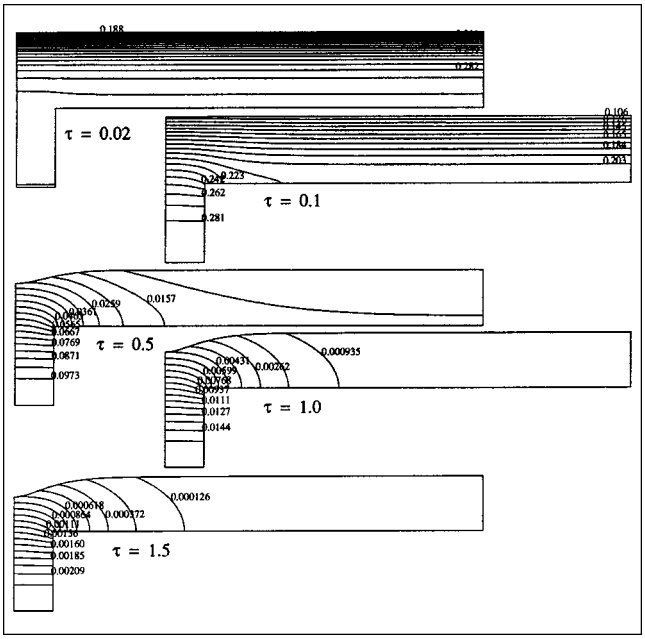

Figure 7. Drying coating over an uneven substrate.

Concentration contour plots and domain boundaries at five intermediate times $\tau = 0.02$, $\tau = 0.1$, $\tau = 0.5$, $\tau = 1$, $\tau = 1.5$. Parameters are $f_s^0 = 0.3$, $f_s^{eq} = 0$, $Sh = 5$, $\Delta\tau = 0.01$, $k/G = \infty$.

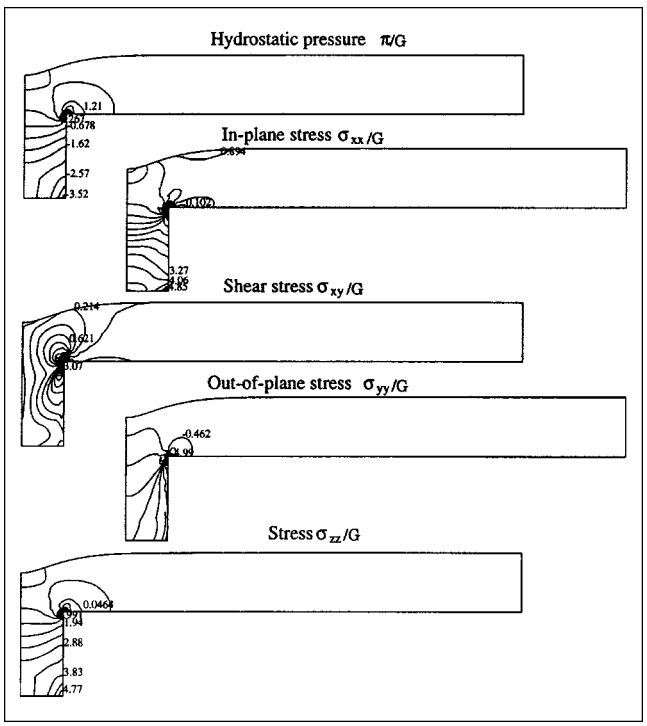

Figure 8. Drying coating over an uneven substrate.

Contour plots of hydrostatic pressure and Cauchy stresses at $\tau = 1$. The units of pressure and stresses are shear modulus. Parameters are $f_s^0 = 0.3$, $f_s^{eq} = 0$, $Sh = 5$, $\Delta\tau = 0.01$, $k/G = \infty$.

Embedded cylinders

The second example shows how the addition of deformable particles into the coating can affect the drying and stress development. In a lot of industrial coating practice, particles are indeed added to polymer solutions to achieve mechanical strength or impart unique properties. For example, magnetic particles (nearly rigid, compared with the coating) are added to solutions and coated on substrates to make floppy disks for magnetic recording. In the photographic industry, silver halide particles are combined with gelatin to make photographic films, and matte particles are used to provide surface roughness that enhances film winding and conveyance. In addition to particles added intentionally to achieve certain functional purposes, unwanted particles may come from a contaminant in the air stream impinging on a wet coating. Particles, either added intentionally or deposited from air, are usually responsible for many defects, among them spots, "starry night" (Gutoff and Cohen, 1995) and edge delamination. The effect of rigid particles on drying and stress in elastic coatings has been studied by Tam (1997) and Christodoulou et al. (1998). Here, their analysis is extended to soft particles where the relaxation effect of stresses around particles is considered as the elasto-viscoplastic coating dries.

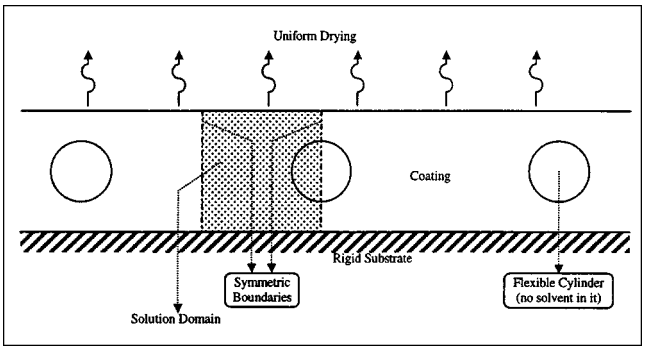

Figure 9. Cylinders embedded in the coating.

Deformable cylinders are spaced periodically in the middle of the coating. The solvent cannot penetrate into the cylinders. Due to the symmetry of the situation, the equations need to be solved only in the shadowed area.

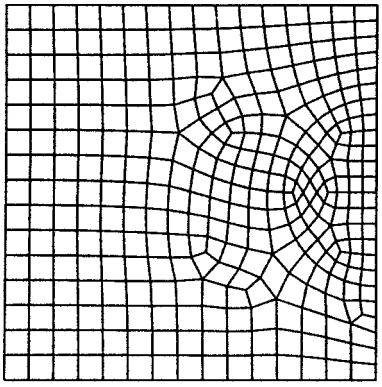

Figure 10. Polymer mesh in solution domain.

The domain is divided into 314 biquadratic nine-node elements with 1,327 nodes. Both the height and the length of the domain are 1 μm, and this characteristic length is used in dimensional analysis. FASTQ, a Sandia-made mesh generator, was used to generate this mesh.

Cylinders periodically distributed in an infinitely long coating are considered (Figure 9). Initially, these cylinders sit halfway between the free convective surface and the substrate/coating interface. Polymer adjacent to the coating/cylinder interface does not slip relative to that surface and moves with it during drying. Neither solvent nor polymer can diffuse into the cylinder and the volume of the cylinder is constant. The substrate is rigid and impermeable to both solvent and polymer. Due to the periodic placement of the particles, all that needs to be found is a solution in the shadow area between two neighboring symmetric planes (see Figure 9).

Two materials with different properties are within the domain. The coating itself has two components that interdiffuse. The cylinder, however, consists of a single nondiffusing component. The coating has the same elasto-viscoplastic behavior as in the previous example. The cylinder, however, is purely elastic. The elastic behavior of both is described by neo-Hookean constitutive relations, but with different shear moduli. In order to simplify programming, an auxiliary variable of solvent volume fraction was assigned to every node within the cylindrical domain, but both that variable and the diffusion coefficient in the cylinder were kept zero at all times. The interface between coating and cylinder is represented by a set of single nodes at which the solvent volume fraction is that of the coating side. In comparison with the double-noded interfaces employed by Schunk and Rao (1994), the single-noded boundary has certain advantages, such as ease in imposing continuity of displacement and traction across the interface, conditions that are implicit in using the single-noded interface.

Two cases with different moduli of the cylinder are represented below. In the first case, the modulus of the cylinder is 100 times that of the coating; this is, to simulate the situation when rigid particles such as silver halide or magnetic particles are present in the coating. In the second case, the cylinder has exactly the same modulus as the coating. This simulates the situation when soft particles are present.

The domain is divided into 314 biquadratic nine-node elements with 1,327 nodes as in Figure 10. Initially, at solidification, there is 30% solvent by volume in the coating. The air swept over the coating is solvent free so that, at final equilibrium, the solvent volume fraction in the coating is zero. The Sherwood number in the following cases is $Sh = 5$ and the unit of stress is the modulus of the coating. The yield stress of the coating is $k = 0.01$ G, a low value. A constant time step of $\Delta\tau = 0.005$ is applied in the Euler backward time integration. $N_{El} = 4$ is used to describe the viscoplastic relaxation behavior after coating yields.

The solvent concentration distributions at five different times $\tau = 0.05$, $\tau = 0.1$, $\tau = 0.15$, $\tau = 0.35$, and $\tau = 0.75$ are shown in Figure 11. As the solvent evaporates from the top of the surface, the coating dries first nearby, and then the drying front propagates into the coating. Because the volume of the cylinder is fixed and its deformation is small compared with that of the coating, the free surface above the particle protrudes. Solvent beneath the cylinder must diffuse around the cylinder in order to reach the free surface and evaporate. Because the diffusion path is longer than in the coating between cylinders, it takes longer to dry the coating beneath the cylinders. At time $\tau = 0.75$, only 5.7 vol. % solvent remains—the coating is close to dry. Thereafter, the coating profile changes little.

Initially, the whole coating is at the concentration of solidification and the stress is zero everywhere. The stress rises in the coating as the coating continues to dry. The evolution of pressure $\bar{\pi}$ and in-plane stress $\bar{\sigma}_{xx}$ is shown in Figure 12. The gradient of the pressure $\bar{\pi}$ is steep near the interface between the coating and cylinder. The in-plane stress is high in the coating atop the cylinder. As the stress rises, its second invariant Φ may locally exceed the yield stress which by hypothesis here is independent of solvent concentration. How the stress evolves after the local stress-free state yields depends on the extent of viscoplastic change of the stress-free state, for that change lowers the subsequent elastic strain and can relax some of the stress in the final state. Thus, during drying of the coating, there is competition between stress development and stress relaxation. In the early stages, drying is rapid, especially near the free surface, and stress development dominates. With the parameters as in Figure 12, the stress is most severe at about $\tau = 0.15$, at which high stress is

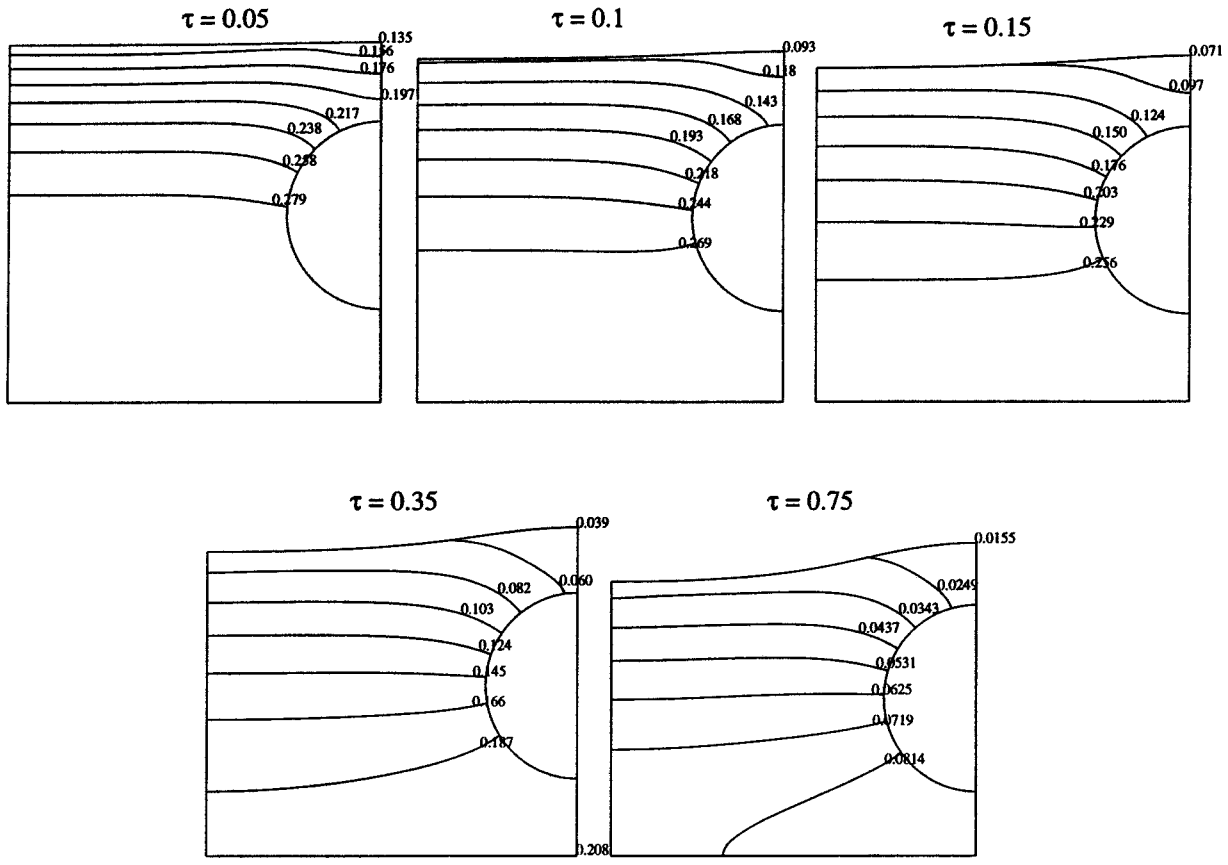

Figure 11. Evolution of solvent volume fraction in the case of nearly rigid cylinders (the cylinder shear modulus is 100 times that of the coating).

Parameters are $f_s^0 = 0.3$, $f_s^{eq} = 0$, $Sh = 5$, $\Delta\tau = 0.005$. For the coating, $k/G = 0.01$ and $N_{El} = 4$; for the cylinders $k/G = \infty$.

most widely distributed. After that, drying slows down and as long as yielding continues, stress evolution is dominated by stress relaxation, so that the regime of high stress recedes.

The modulus of the cylinder in the coating can affect the stress distribution. When it has the same modulus as the coating itself, the in-plane stress evolves as shown in Figure 13. The in-plane tensile stress acts on the interface between the cylinder and the coating, pulling on and elongating the deformable cylinder. As a result, the free surface profile becomes more nearly flat than that of Figure 12, the case of a nearly rigid cylinder. The stress near the soft cylinder is smaller than that near the rigid one. Consequently, stress-induced defects are likely to be less severe than those induced by rigid cylinders.

Cantilever deflection

The last example is the deflection of a cantilever bearing a drying or curing coating. This is the configuration used in the measurement of stress in experiments by Croll (1978), Perera and Eynde (1981), and recently by Payne (1998). In their experiments, solvent solution (polymer solution, gelatin, UV-curable solution) is coated on one side of a thin steel (sometimes silicon) substrate. During drying or curing, in-plane stress develops in the coating and causes the composition of coating and substrate to bend toward the coating side. From the amount of deflection and the coating thickness, the in-plane stress can be derived (Corcoran, 1969).

Two materials are within the domain coating and substrate. The coating has two components that interdiffuse, and has the same elasto-viscoplastic behavior as in previous examples. The substrate, however, consists of a single nondiffusing component, and is purely elastic. Just as with drying embedded cylinders, an auxiliary variable of solvent volume fraction was assigned to every node within the substrate domain, but both that variable and the diffusion coefficient in the substrate were kept zero at all times. The interface between coating and substrate is represented by a set of single nodes at which the solvent volume fraction is that of the coating side.

The case considered is shown in Figure 14. It is a strip 180 μm long by 8 μm thick on which a 9 μm thick coating is applied. The shear modulus of the coating is used as the unit of stress, and a characteristic length of 100 μm is used as the unit of length. This domain (both coating and flexible substrate) is divided into 1,281 nodes and 300 biquadratic elements, among which 180 elements are in the coating and the rest in the substrate (Figure 15). At the clamped end of the domain, material can only move vertically and thus the sym-

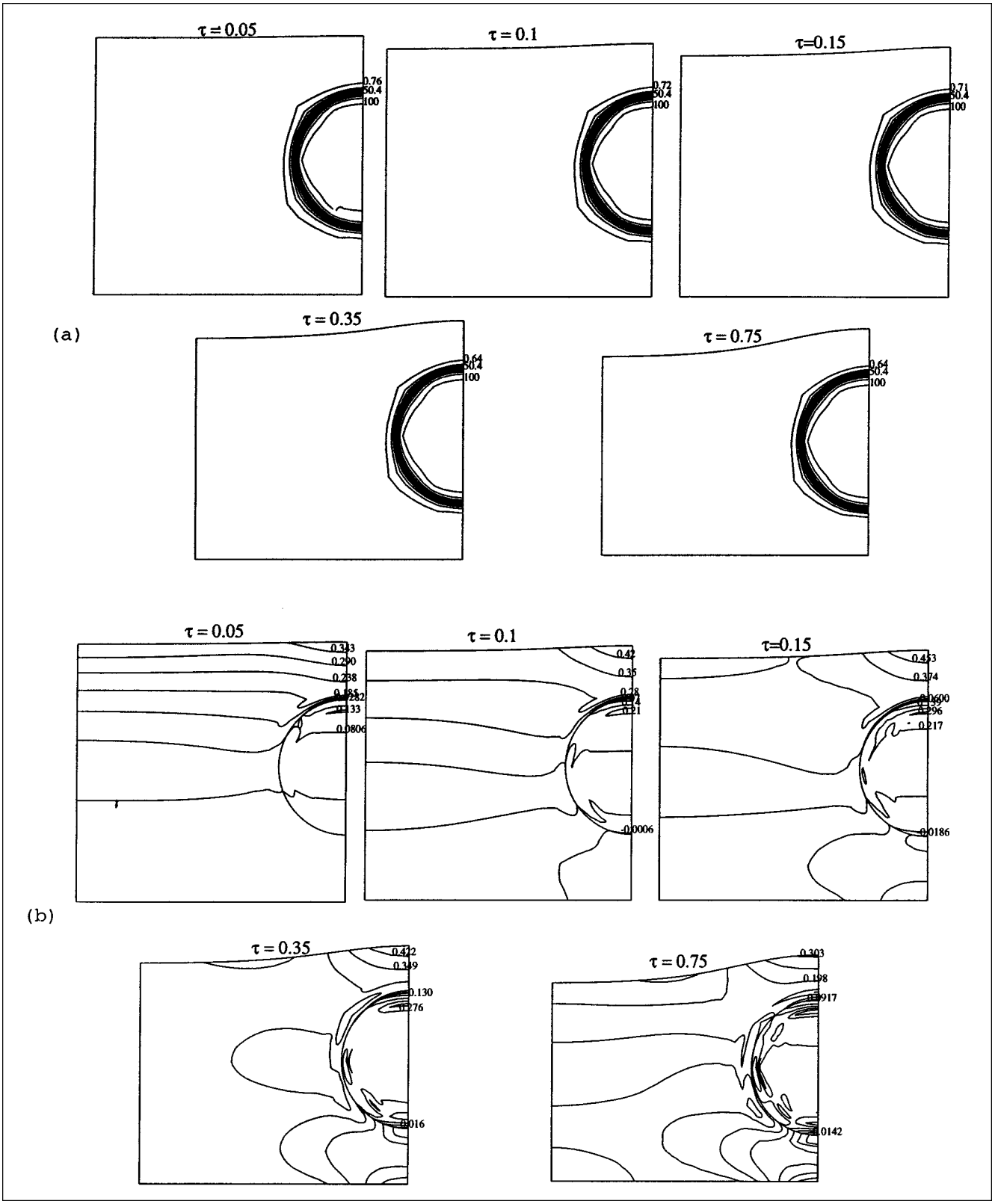

Figure 12. Evolution of pressure like-parameter $\bar{\pi}$ (a) and in-plane stress $\bar{\sigma}_{xx}$ (b) in the case of nearly rigid cylinders (cylinder has a shear modulus 100 times that of the coating).

The smoothing technique (Lee et al., 1979) is not applied. Parameters are $f_s^0 = 0.3$, $f_s^{eq} = 0$, $Sh = 5$, $\Delta\tau = 0.005$, $k/G = 0.01$, $N_{El} = 4$ for the coating, and $k/G = \infty$ for cylinders.

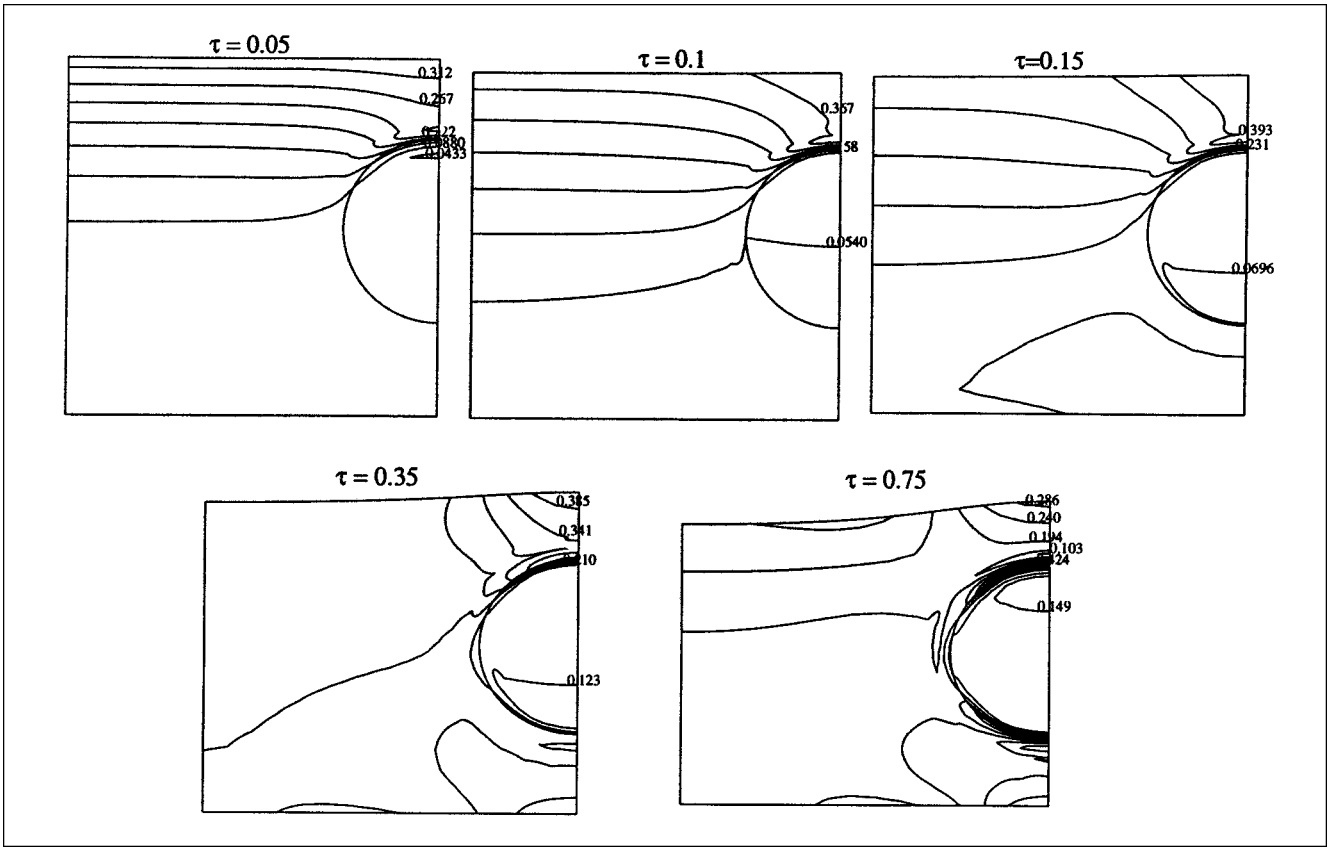

Figure 13. Evolution of in-plane stress $\bar{\sigma}_{xx}$ in the case of nearly soft cylinders (cylinder has the same modulus as that of the coating).

Parameters are $f_s^0 = 0.3$, $f_s^{eq} = 0$, $Sh = 5$, $\Delta\tau = 0.005$, $k/G = 0.01$, $N_{El} = 4$ for the coating, and $k/G = \infty$ for cylinders.

metry condition is applied in which the horizontal movement is constrained. The substrate is impermeable to both the solvent and the polymer particles.

Figure 16 shows the evolution of solvent concentration in the coating as the cantilever deflects upward when the cantilever has a modulus 10 times that of the coating. The coating is initially in its stress-free state and, at solidification, has a uniform solvent distribution. The initial solvent concentration is 30% by volume. The final solvent concentration, when the solvent in coating is in equilibrium with that in the air, is zero. The Sherwood number $Sh = 5$ and a constant time step of $\Delta\tau = 0.001$ is used. The coating is modeled as elasto-viscoplastic material whose elasticity number $N_{El} = 4$ and yield stress $k = 0.01$G, with G being the coating modulus that is used as the unit of stress. As shown in Figure 16, the solvent depletes first at the upper lefthand side corner where it evaporates from both the top and the edge. From the concentration contour plots, the distance from the edge over which the edge effect reaches is remarkable, much longer than three coating thickness, over which the edge has an effect on

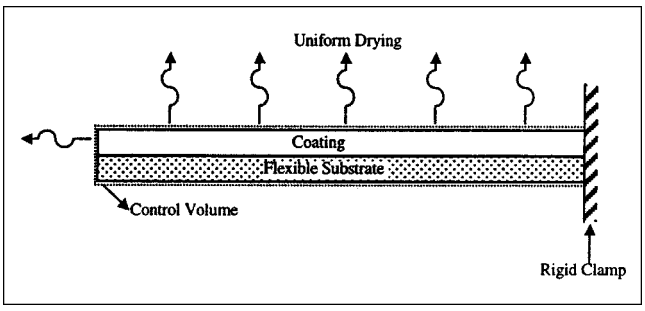

Figure 14. Example used to analyze cantilever deflection: a 9 μm coating is applied onto an 8 μm thick and 180 μm long substrate.

The characteristic length of 100 μm is used in dimensional analysis.

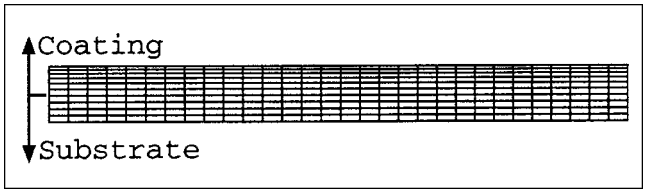

Figure 15. Polymer mesh in computational.

The domain is divided into 300 biquadratic nine-node elements with 1,281 nodes. The interface between coating and substrate is represented by a set of single nodes at which the solvent volume fraction is that of the coating side.

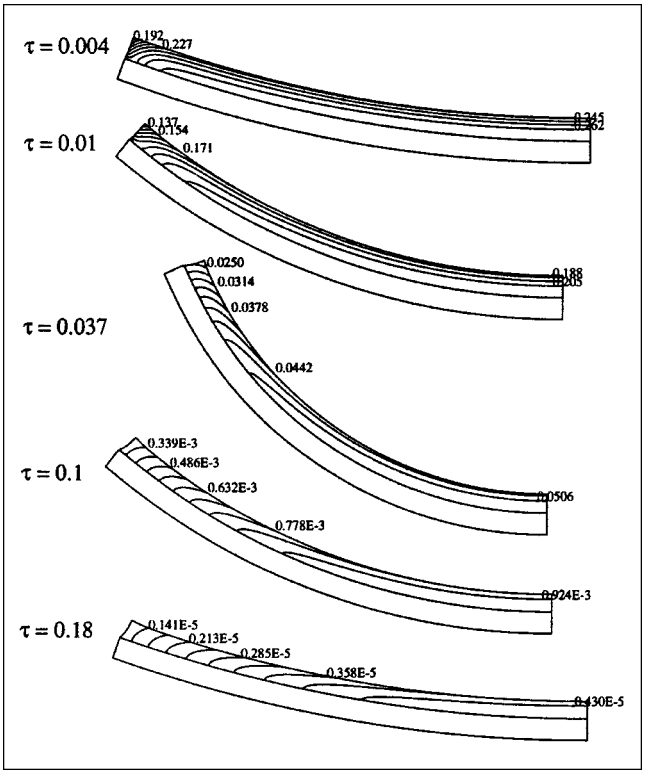

Figure 16. Evolution of solvent concentration in the coating coated on a flexible substrate.

The coating/substrate interface is impermeable to both polymer and solvent. The modulus of the substrate is 10 times that of the coating. Parameters are $f_s^0 = 0.3$, $f_s^{eq} = 0$, $Sh = 5$, $\Delta\tau = 0.001$, $k = 0.01\ G$, $N_{El} = 4$ for coating, and $k/G = \infty$ for substrate.

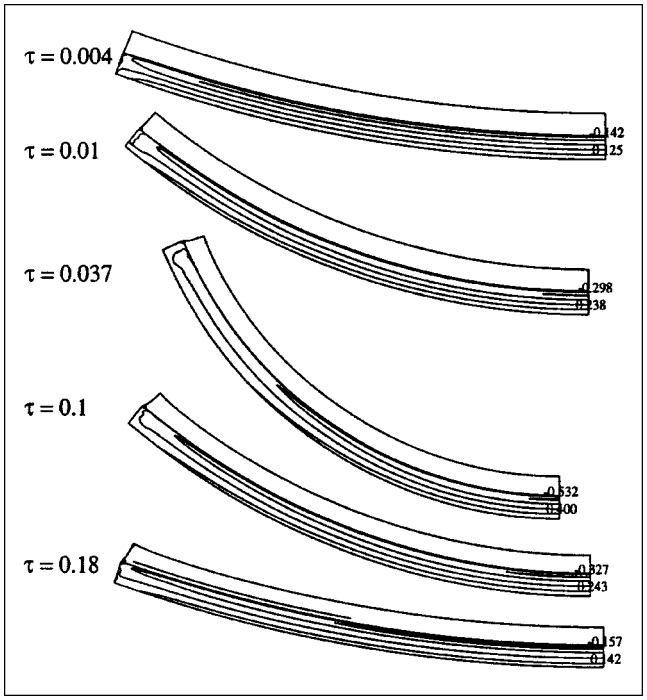

Figure 17. Evolution of in-plane stress $\bar{\sigma}_{xx}$ in the substrate.

The modulus of the substrate is 10 times that of the coating. Parameters are $f_s^0 = 0.3$, $f_s^{eq} = 0$, $Sh = 5$, $\Delta\tau = 0.001$, $k = 0.01G$, $N_{El} = 4$ for coating, and $k/G = \infty$ for substrate.

stress. The stress in Figure 17 is in units of the coating modulus, which is only one-tenth of the substrate modulus. As the drying continues, the in-plane stress rises more and more, and so does the deflection of the cantilever. However, once the local stress in the coating exceeds the local yield stress, the stress relaxes upon viscoplastic deformation. As a result of stress relaxation, the cantilever deflection decreases.

It should be noted that large deflections, as shown in Figures 16 and 17, can only be seen while the coating is coated on a flexible substrate. Large deflections were observed experimentally by Payne (1998) when a polystyrene-toluene solution was coated on a flexible polyethylene terephthalate (PET) substrate. For most cantilever devices where steel substrate is used for stress measurement, the deflections are usually significantly smaller. The model above is also capable of predicting these small deflections.

Summary

Stress development in a shrinking coating is due to the nonuniform shrinkage as coating dries, and the inherence of in-plane shrinkage from the substrate on which it is coated. The study presented here focuses on the drying after coating solidifies, in which the coating is considered as an elasto-viscoplastic material and it starts drying from the stress-free solidification point. The theories are developed for Fickian diffusion, kinematics of volume shrinkage, elastic deformation, viscoplastic flow, and the related stress development as the polymer coating dries. The elastic behavior is modeled with the neo-Hookean large deformation constitutive relation. The start of plastic yielding is predicted by Von Mises' yield criterion without strain hardening. After yielding, the rate of stress relaxation is proportional to the excess stress above the yield surface, and it changes in the direction normal to yield surface in the stress space.

The Galerkin/finite element method is applied to solve the full equation system. This model is then used to study the effect of uneven substrate and embedded particles on the drying and stress development in coatings. Solutions show the changes in solvent concentration, pressure, viscous stress, and surface topography as coating dries further after solidification. The model is then used to simulate the deflection of a cantilever substrate coated with polymer solution on one side.

Acknowledgments

This research was supported by the Center for Interfacial Engineering, a NSF sponsored Engineering Research Center at the University of Minnesota, through its Coating Process Fundamentals Program. We are grateful to K. S. A. Chen, S.-Y. Tam, J. A. Payne, and S. Weinstein for helpful discussions.

Literature Cited

Billovits, G. F., and C. J. Durning, "Polymer Material Coordinates for Mutual Diffusion in Polymer Penetrant Systems," *Chem. Eng. Commun.*, **82**, 21 (1989).

Bornside, D. E., "Spin Coating," PhD Thesis, Univ. of Minnesota (1988).

Bornside, D. E., "Mechanism for the Local Planarization of Microscopically Rough Surfaces by Drying thin Films of Spin-Coated Polymer/Solvent Solutions," *J. Electrochem. Soc.*, **137**, 2589 (1990).
Cairncross, R. A., L. F. Francis, and L. E. Scriven, "Competing Drying and Reaction Mechanisms in the Formation of Sol-to-Gel Films, Fibers, and Spheres," *Drying Technol.*, **10**, 893 (1992).
Christodoulou, K. N., E. J. Lightfoot, and R. W. Powell, "Model of Stress-Induced Defect Formation in Drying Polymer Films," *AIChE J.*, **44**, 1484 (1998).
Corcoran, E. A., "Determining Stresses in Organic Coatings Using Plate Beam Deflection," *J. Paint Technol.*, **41**, 635 (1969).
Crank, J., *The Mathematics of Diffusion*, Clarendon Press, Oxford (1975).
Croll, S. G., "Internal Stress in a Solvent-Cast Thermoplastic Coating," *J. Coat. Tech.*, **50**, 33 (1978).
Croll, S. G., "The Origin of Residual Internal Stress in Solvent-Cast Thermoplastic Coatings," *J. Appl. Polym. Sci.*, **23**, 847 (1979).
Dafalias, Y. F., "The Plastic Spin," *J. Appl. Mech.*, **52**, 865 (1985).
Durning, C. J., "Mutual Diffusion in Concentrated Polymer Solutions Under a Small Driving Force," *Macromolecules*, **19**, 2220 (1986).
Gutoff, E. B., and E. D. Cohen, *Coating and Drying Defects: Troubleshooting Operation Problems*, Wiley, New York (1995).
Hasatani, M., and Y. Itaya, "Fundamental Study on Shrinkage of Formed Clay During Drying-Viscoelastic Strain-Stress and Heat/Moisture Transfer," *Drying Technol.*, **10**, 1013 (1992).
Hasatani, M., Y. Itaya, and K. Muroie, "Contraction Characteristics of Molded Ceramics During Drying," *Drying Technol.*, **11**, 815 (1993).
Irudayaraj, J., and K. Haghighi, "Stress Analysis of Viscoelastic Materials During Drying," *Drying Technol.*, **11**, 901 (1993).
Itaya, Y., S. Mabuchi, and M. Hasatani, "Deformation Behavior of Ceramics Slabs by Nonuniform Drying," *Drying Technol.*, **13**, 801 (1995).
Larche, F. C., and J. W. Cahn, "A Linear Theory of Thermochemical Equilibrium of Solids Under Stress," *Acta. Metall.*, **21**, 1051 (1973).
Larche, F. C., and J. W. Cahn, "The Effect of Self-Stress on Diffusion in Solids," *Acta. Metall.*, **30**, 1835 (1982).
Lee, E. H., "Elastic-Plastic Deformation at Finite Strains," *J. Appl. Mech.*, **91**, 1 (1969).
Lee, R. L., P. M. Gresho, and R. L. Sani, "Smoothing Techniques for Certain Primitive Variable Solutions of the Navier-Stokes Equation," *Int. J. Num. Meth. Eng.*, **14**, 1785 (1979).
Lei, H., "Flow, Deformation, Stress and Failure in Solidifying Coatings," PhD Thesis, Univ. of Minnesota (1999).
Lei, H., J. A. Payne, L. F. Francis, A. V. McCormick, W. W. Gerberich, and L. E. Scriven, "Stress Development in Drying Coatings," *J. Appl. Poly. Sci.*, **81**, 1000 (2001).
Li, J. C. M., R. A. Oriani, and L. S. Darken, "The Thermodynamics of Stressed Solids," *Z. Physik. Chem. Neue Folge*, **49**, 271 (1966).
Li, J. C. M., "Chemical Equilibrium in a Stressed Polymers," *J. Appl. Phys.*, **42**, 4543 (1971).
Lubliner, J., *Plasticity Theory*, Macmillan, New York (1990).
Malvern, L. E., *Introduction to the Mechanics of a Continuous Medium*, Prentice-Hall, Englewood Cliffs, NJ (1969).
Moran, B., M. Ortiz, and C. F. Shih, "Formulation of Implicit Finite Element Methods for Multiplicative Finite Deformation Plasticity," *Int. J. Num. Meth. Eng.*, **29**, 483 (1990).
Owen, D. R. J., and E. Hinton, *Finite Elements in Plasticity: Theory and Practice*, Pineridge Press Ltd., Swansea, U. K. (1980).
Payne, J. A., "Stress Evolution in Solidifying Coatings," PhD Thesis, Univ. of Minnesota (1998).
Perera, D. Y., and D. V. Eynde, "Considerations on a Cantilever (Beam) Method for Measuring the Internal Stress in Organic Coatings," *J. Coat. Tech.*, **53**(677), 39 (1981).
Peurrung, L. M., and D. B. Graves, "Film Thickness Profiles over Topography in Spin Coating," *J. Electrochem. Soc.*, **138**, 2115 (1991).
Rivlin, R. S., and D. W. Saunders, "Large Elastic Deformations of Isotropic Materials: Experiments on the Deformation of Rubber," *Phil. T. Roy. A*, **243**, 251 (1951).
Schunk, P. R., and R. R. Rao, "Finite Element Analysis of Multi-Component Two-Phase Flows with Interphase Mass and Momentum Transport," *Int. J. Num. Meth. Fluids*, **18**, 821 (1994).
Tam, S. Y., L. E. Scriven, and H. K. Stolarski, "Stress Effects in Drying Polymer Films," *Mater. Res. Soc. Symp. Proc.*, **356**, 547 (1995).
Tam, S. Y., "Stress Effects in Drying Coatings," PhD Thesis, University of Minnesota (1997).
Vergne, D. B. L., and D. C. Hofer, "Modeling Planarization with Polymers," *Proc. Soc. Photo.*, **539**, 115 (1985).
White, L. K., "Planarization Properties of Resist and Polyimide Coatings," *J. Electrochem. Soc.*, **130**, 1543 (1983).
Wilson, R. H., and P. A. Piacente, "Effect of Circuit Structure on Planarization Resist Thickness," *J. Electrochem. Soc.*, **133**, 981 (1986).
Wu, Q., and M. R. Milota, "Effect of Creep and Mechano-Sorptive Effect on Stress Development During Drying," *Drying Technol.*, **12**, 2057 (1994).

Manuscript received Aug. 21, 2000, and revision received Sept. 10, 2001.